PHOTONICS Research

$Ge_{0.92}Sn_{0.08}$/Ge multi-quantum-well LEDs operated at 2-μm-wavelength on a 12-inch Si substrate

Shaoteng Wu,[1,2,5] Lin Zhang,[1] Rongqiao Wan,[1,6] Hao Zhou,[1] Kwang Hong Lee,[1] Qimiao Chen,[1,7] Yi-Chiau Huang,[3] Xiao Gong,[4] and Chuan Seng Tan[1]

[1]School of Electrical and Electronic Engineering, Nanyang Technological University, Singapore 639798, Singapore
[2]State Key Laboratory of Superlattices and Microstructures, Institute of Semiconductors, Chinese Academy of Sciences, Beijing 100083, China
[3]Applied Materials, Inc., Sunnyvale, California 95054, USA
[4]Department of Electrical and Computer Engineering, National University of Singapore, Singapore 117576, Singapore
[5]e-mail: shaoteng.wu@ntu.edu.sg
[6]e-mail: rongqiao.wan@ntu.edu.sg
[7]e-mail: chenqm@ntu.edu.sg

Received 29 March 2023; accepted 17 July 2023; posted 19 July 2023 (Doc. ID 491763); published 12 September 2023

The development of an efficient group-IV light source that is compatible with the CMOS process remains a significant goal in Si-based photonics. Recently, the GeSn alloy has been identified as a promising candidate for realizing Si-based light sources. However, previous research suffered from a small wafer size, limiting the throughput and yield. To overcome this challenge, we report the successful growth of GeSn/Ge multiple-quantum-well (MQW) p-i-n LEDs on a 12-inch (300-mm) Si substrate. To the best of our knowledge, this represents the first report of semiconductor LEDs grown on such a large substrate. The MQW LED epitaxial layer is deposited on a 12-inch (300-mm) (001)-oriented intrinsic Si substrate using commercial reduced pressure chemical vapor deposition. To mitigate the detrimental effects of threading dislocation densities on luminescence, the GeSn/Ge is grown pseudomorphically. Owing to the high crystal quality and more directness in the bandgap, enhanced electroluminescence (EL) integrated intensity of 27.58 times is demonstrated compared to the Ge LED. The MQW LEDs exhibit EL emission near 2 μm over a wide operating temperature range of 300 to 450 K, indicating high-temperature stability. This work shows that GeSn/Ge MQW emitters are potential group-IV light sources for large-scale manufacturing.

https://doi.org/10.1364/PRJ.491763

1. INTRODUCTION

Due to their scalable inclusion with current Si CMOS techniques, group IV semiconductors are appealing for photonics applications [1]. To build up a full set of components for Si photonics, numerous optoelectronic devices, such as amplifiers, modulators, waveguides, couplers, switches, photodetectors, LEDs, and lasers, should be included. However, even though most optoelectronic devices have been fully realized, the realization of effective group-IV light sources (LEDs, lasers) is still a challenge as Si and Ge are indirect band materials [2–4]. Recently, group-IV GeSn material has been suggested as a potential direct bandgap alloy for Si-based light sources [5–7]. GeSn alloy LEDs and optically/electronically pumped GeSn lasers have been experimentally demonstrated from several groups [5,8–10]. With remarkable enhancement of recombination efficiency, the multiple-quantum-well (MQW) structure has been widely used on LEDs or lasers, and some GeSn/Ge or GeSn/SiGeSn/MQW structure emitters have also been reported [11–13]. However, the previous MQW GeSn LEDs suffer from small wafer sizes, which leads to low throughput and yield. Moreover, to the best of our knowledge, previously reported semiconductor LEDs all have a wafer diameter ≤8 inches (200 mm).

Today, there are imperious demands for Si-based optoelectronic devices at wavelengths of around 2 μm (1900–2100 nm), due to wide applications in biomedical sensing, gas sensing (especially CO_2 sensors), and 3D light detection and ranging (LiDAR) [14]. Furthermore, due to the rapid progress in hollow-core photonic bandgap fibers (HC-PBGFs), a lowest-loss window at ∼2 μm has been found recently, which opens a promising window for communication applications at 2 μm [15,16]. High-speed (>10 GHz) Si-based GeSn photodetectors at the waveband of 2 μm have been realized [17–19], but the corresponding efficient Si-based light source is still a challenge. On the other hand, there are also demands for investigations of high-temperature stability (300–450 K) of GeSn LEDs for the following reasons: (1) ease of Sn segregation at high temperatures for GeSn alloys [20–22]; (2) GeSn light emitter might have high electroluminescence (EL) intensity at elevated temperatures [23]; (3) due to the Joule heating effect,

the operating temperature for Si integrated circuits can reach 150°C (423 K) [24].

Here, we present the first p-i-n semiconductor LEDs on the 12-inch (300 mm) substrate. The MQW GeSn/Ge LEDs were grown on a 12-inch (300 mm) (001) Si substrate by a commercial reduced pressure chemical vapor deposition (RPCVD) system using a 1.2-μm Ge buffer layer, indicating enormous potential for large-scale manufacturing. The EL characterization of GeSn/Ge MQW LEDs under different current injections was studied. EL from MQW LEDs was observed near 2 μm with a high operating temperature around 450 K. The temperature-dependent EL and photoluminescence (PL) emissions of the MQW LEDs were also studied.

2. RESULTS AND DISCUSSION

A. Material Growth and Characterization

The GeSn/Ge MQW LEDs were grown on the 12-inch (300 mm) Si substrate by a commercial RPCVD system [25]. To reduce the lattice mismatch between GeSn and Si, a 1.2-μm strain-relaxed Ge layer was used as a buffer layer, which confines the defects near the Ge and Si interface. *In situ* doping was adopted to grow the p-type and n-type Ge contact layers (~200 nm). GeSn/Ge MQW layers consist of 15 periods of $Ge_{0.92}Sn_{0.08}$ well layer and Ge barrier layer with thicknesses of 7.5 and 20 nm, respectively, grown at a temperature of below 350°C. The thin GeSn well layers were deliberately designed to provide better carrier confinement for excitons and to inhibit dislocation formation from strain relaxation. The cross-sectional transmission electron microscope (TEM) image in Fig. 1(a) shows the abrupt and uniform interfaces on the GeSn and Ge layers. Furthermore, dislocations observed near the Ge/Si interfaces also demonstrate the high crystal quality of MQW layers. The high-resolution TEM (HRTEM) image on the MQW region in Fig. 1(b) shows that the Ge and GeSn layers are single crystals without observable dislocations.

The Sn content and strain of GeSn/Ge MQWs were characterized by X-ray diffraction (XRD). The 2Theta-Omega curve along the (004) direction of the as-grown sample shows Si, Ge, and GeSn peaks (right to left). Plenty of satellite peaks exist on the left of the Ge peak, indicating the uniform and high crystalline quality of the GeSn/Ge MQW structure. The reciprocal space mapping (RSM) along (224) orientation is shown in Fig. 1(d). As expected, the same reciprocal lattice vector Q_x of the Ge and diffraction GeSn peaks demonstrates that the GeSn layers are pseudomorphically grown. The pseudomorphic growth of the GeSn/Ge will not introduce additional threading dislocations (TDs) in the wafer, which will act as a non-radiative recombination center conducive to luminescence. Based on the RSM, the Sn content and strain of the GeSn are calculated to be about 8% and 0.0116%, respectively.

B. Band Alignment Calculation

The band alignments of the GeSn/Ge MQW were studied using model-solid theory [19,25]. According to Vegard's law, $E_g(Ge_{1-x}Sn_x) = (1-x)E_g(Ge) + xE_g(Sn) - b^{GeSn}(1-x)x$, where

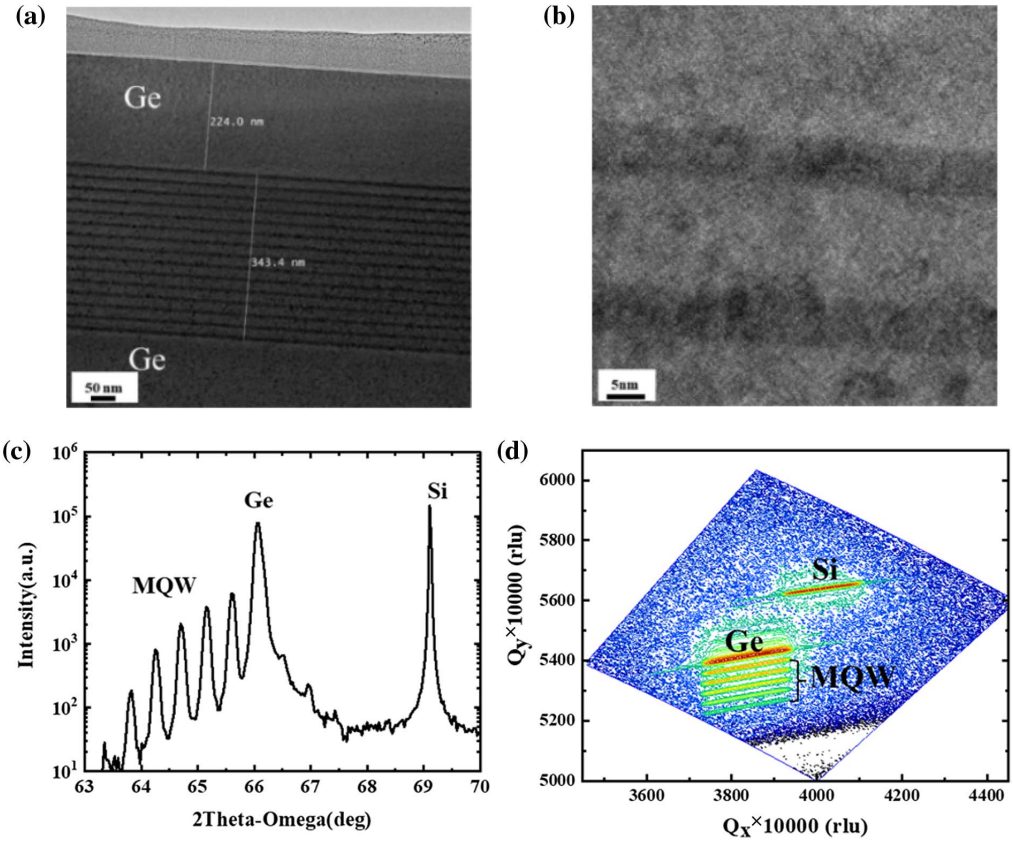

Fig. 1. (a), (b) TEM and HRTEM images of the GeSn/Ge MQW structure on 12-inch Si substrate. (c), (d) High-resolution XRD 2Theta-Omega curve and asymmetric (224) XRD-RSM of the as-grown sample.

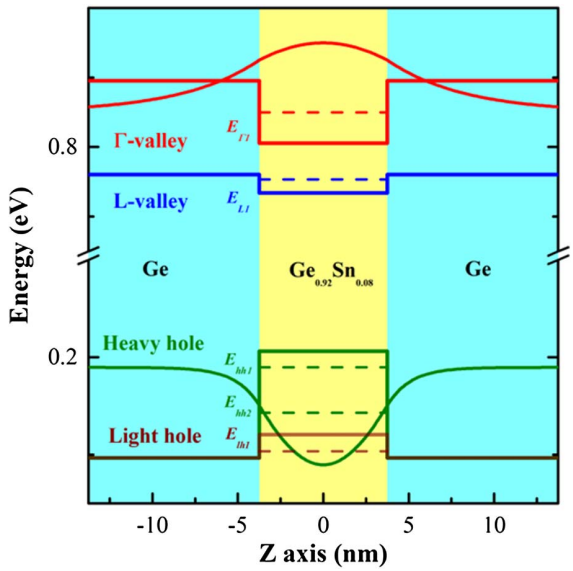

Fig. 2. Band alignments of the GeSn/Ge MQW.

x and b^{GeSn} are the Sn content and bowing parameter, respectively, and the bandgap of the GeSn without strain was calculated. From the deformation potential theory, the energy shifts due to strain can be expressed, where the strain value was obtained from the above XRD-RSM measurement. The band alignment of the GeSn/Ge MQW LED is shown in Fig. 2. The calculation shows that the GeSn well is an indirect bandgap material and the MQW is type I band alignment. The barrier offsets for electrons in Γ-valley and L-valley (ΔE_{Γ} and ΔE_{L}) are 89.6 and 26.8 meV, and for holes in heavy hole and light hole bands (ΔE_{HH} and ΔE_{LH}) are 109.6 and 24.0 meV, respectively. Additionally, due to the Sn substitution, the bandgap between the Γ-valley and L-valley is reduced from 134.5 meV (unstrained Ge) to 71.7 meV ($Ge_{0.92}Sn_{0.08}$).

As the active GeSn layers are in a quantum well structure, the quantum confinement effect should be considered. The ground states of bands in the GeSn well were calculated from the 1D time-independent Schrödinger equation

$$-\frac{h^2}{8\pi^2 m^*(z)}\frac{\partial^2 \psi_n}{\partial z^2} + V(z)\psi_n = E_n\psi_n, \tag{1}$$

where h, $m^*(z)$, $V(z)$, ψ_n, and E_n are the Planck constant, effective mass of electrons (holes), band offsets, eigenfunction, and eigenvalue, respectively. Eventually, the direct bandgap ($E_{\Gamma 1} - E_{\mathrm{hh1}}$) in the GeSn well region is calculated to around 0.660 eV (1880 nm).

C. Device Fabrication and Characterization

GeSn LEDs with double-mesa structures were generated on the epitaxial sample. The 3D image of the GeSn/Ge MQW LED on a Si substrate is shown in Fig. 3(a). To realize the devices, the top mesas were first etched by reactive ion etching (RIE) using chlorine-based gas to reach the p+ Ge region. Subsequently, the bottom mesa was fabricated to isolate the adjacent devices using a similar process. Afterwards, a SiO_2 passivation layer with thickness of 400 nm was deposited by plasma-enhanced chemical vapor deposition (PECVD). After the formation of the contact window by fluorine-based RIE, Ti (20 nm)/Au (200 nm) was deposited by electronic beam evaporation followed by a lift-off process. The top-view microscope image of the fabricated MQW LED is shown in Fig. 3(b).

To characterize the electrical properties of GeSn LEDs, a microprobe station connected to a Keithley 2400 source meter unit (SMU) was used. Figure 3(c) shows the current–voltage (I-V) curve of the GeSn/Ge MQW LED with a 60-μm mesa diameter. The high on/off ratio of $>10^4$ and low dark current under negative voltage both demonstrate the high performance of the Ge/GeSn MQW LEDs. The high on/off ratio of $\sim 10^4$ at ± 1 V demonstrates the excellent rectifying behavior of the GeSn LED. Additionally, the dark current is as low as 0.78 μA at −1 V, corresponding to a current density of 27.58 mA/cm^2. Due to the low threading dislocation densities (TDDs) from the pseudomorphic growth, the dark current density of our device is one of the lowest of GeSn photodiodes with similar Sn content [26,27]. Additionally, the ideal factor η was calculated to ∼1.36 by linearly fitting the slope of the ln$I$-V line. The low ideal factor indicates the LED is close to the ideal PN junction.

The EL characteristics of the GeSn/Ge MQW LEDs were measured by a homemade micro photoluminescence system connected to microprobes for injecting the current. The output EL light was first collected by a 50× objective lens, then propagated to the spectrometer, and finally detected by a liquid nitrogen-cooled linear InGaAs detector array. Limited by the InGaAs detector, the system could measure the accurate PL/EL spectra only within the wavelength of 2030 nm. The room temperature EL spectrum of the GeSn/Ge MQW LED with the comparison of Ge LED is shown in Fig. 3(d). For the accuracy of EL comparison, both LEDs have the same mesa diameter (60 μm) and are under the same injection current (23 mA). Additionally, the i-Ge region of the Ge LED has a thickness of 900 nm to enhance the EL intensity. The Ge LED also has a high crystal quality with TDDs as low as $\sim 10^6$ cm^{-2} [28]. Different from the dominant peak of Ge LED near 0.785 eV (∼1578 nm), the peak of the GeSn LED is redshifted to 0.665 eV (1864 nm), consistent with the theoretical calculation of ∼0.660 eV for the direct bandgap ($E_{\Gamma 1} - E_{\mathrm{hh1}}$) of the GeSn well. The emission of the GeSn LED covers a wide range from 0.65 to 0.85 eV (1458–2066 nm), which covers the S, O, L, U, and 2-μm optical communication bands. Moreover, the integrated EL intensity of the GeSn/Ge MQW LED (red line) is found to be 27.58 times the intensity of the Ge LED (black line). Due to the Sn substitution, the bandgap difference $\Delta E(\Gamma/\mathrm{L})$ between the Γ-valley and L-valley is reduced from 134.5 meV (Ge) to 71.7 meV ($Ge_{0.92}Sn_{0.08}$). As the possibility of electron carriers in L-valley is proportional to $\exp[-\Delta E(\Gamma/\mathrm{L})/kT]$ [29], a remarkable change in emission intensity could be expected. Moreover, the MQW structure with type I band alignment also improves luminescence performance due to the increased carrier restriction. Finally, by Gaussian fitting, the EL spectrum of the GeSn LED was found to comprise four peaks. Peaks 2 and 3 near 0.665 eV (1864 nm) and 0.723 eV (1715 nm) are confirmed to be the direct bands of GeSn/Ge and Ge peaks, respectively, as will be demonstrated from the PL curves below. Peak 1 is mainly from the indirect band of GeSn/Ge, while peak 4 might be due to the

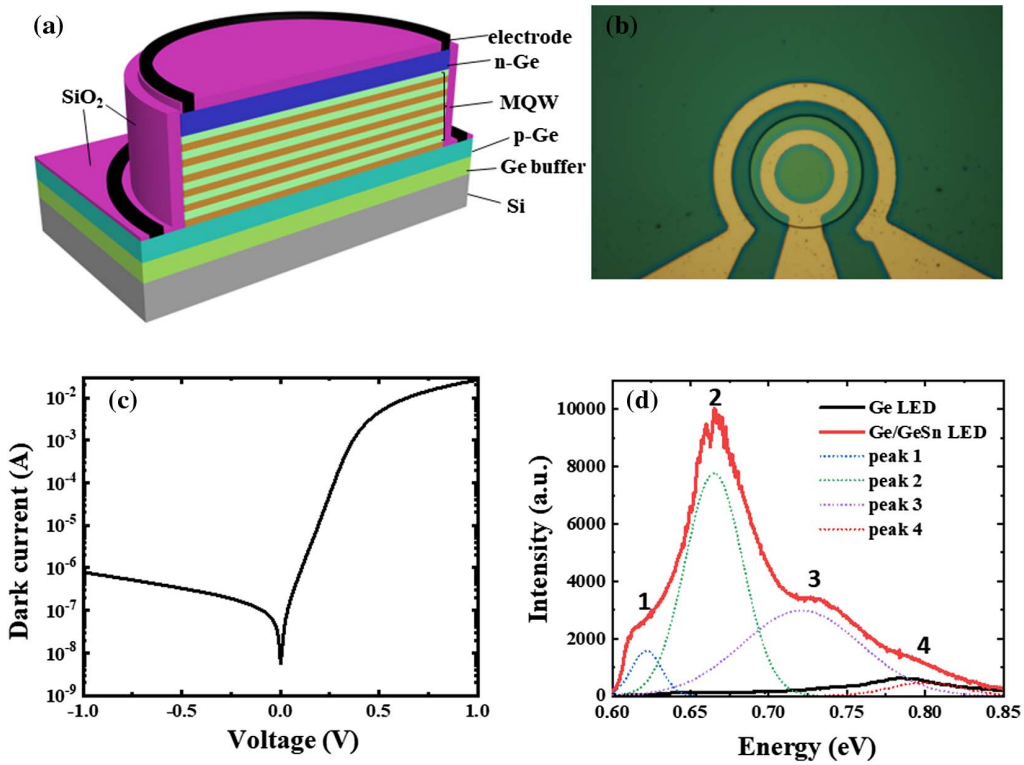

Fig. 3. (a) 3D schematic diagram of the GeSn/Ge MQW LED; (b) top-view microscope image of the fabricated LED; (c) *I-V* characteristics of the LED; (d) room temperature EL spectrum of the GeSn/Ge LED in comparison with that of Ge LED.

Fabry–Perot modes between Ge-VS/Si and Ge/air interfaces [30] or the Ge peak from the buffer Ge layer.

EL spectra at room temperature with injected current ranging from 1 to 50 mA are plotted in Fig. 4(a). The position and intensity of MQW and Ge peaks from EL spectra are extracted and shown in Fig. 4(b). Due to the increasing amount of injected carriers, an obvious EL intensity enhancement is observed on the MQW and Ge peaks from the increase of current. The monotonic increase of integrated EL intensities with the increase of current density in Fig. 4(b) indicates that higher emission could be realized by further increasing the current. On the other hand, it is hard to see any shift in the energy of the MQW peak with increasing injection current, in contrast to an obvious redshift for the Ge peak. The peak of the MQW only shifted from 0.668 to 0.664 eV when the current density increased from 35 to 1768 A/cm^2. In contrast, in the same current density range, the Ge peak has a large redshift from 0.737 to 0.718 eV. A general view suggests that EL peaks will redshift when the injection current increases due to the Joule heating from electrical excitation [31]. By investigating previous reports, a similar phenomenon that the peaks of Ge LEDs are greatly affected while the peaks of GeSn LEDs are hardly shifted from the Joule heating could be concluded [29,32,33]. For quantum well structure LEDs, the injection current increase can also cause band filling effects, which are offset just by thermal effects. This may be the main reason why GeSn EL peaks do not shift. The low radiation recombination efficiency of the Ge LED will result in plenty of heat generation, which might aggravate the Joule heating.

The study of the temperature-dependent EL of LEDs is critical, especially at high temperatures, as it mostly reflects the actual operating environment of the devices. EL spectra

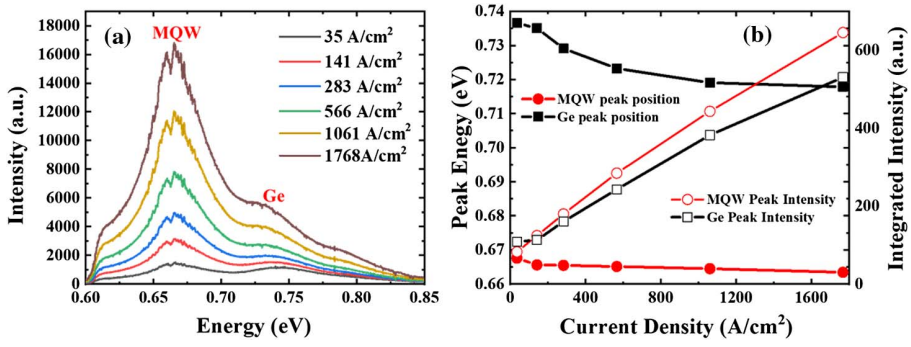

Fig. 4. (a) EL spectra as a function of the injected current; (b) peak position and EL integrated intensity as a function of the current density.

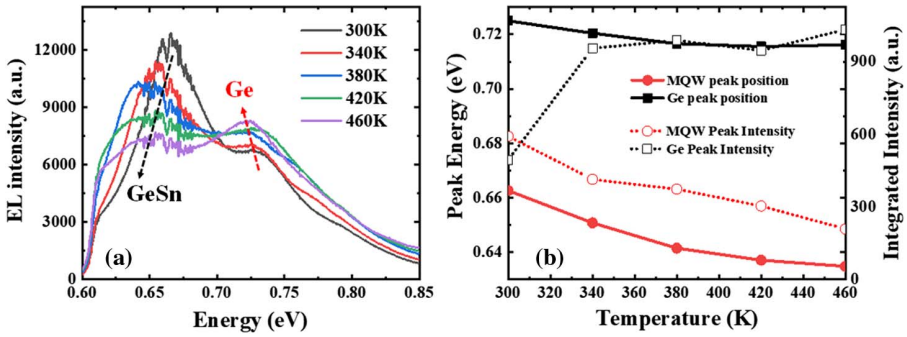

Fig. 5. (a) EL spectra as a function of the temperature for fixed injected current density of ~1900 A/cm^2; (b) peak position and EL integrated intensity at temperature from 300 to 460 K.

at the temperatures from 300 to 460 K under a fixed injected current density of ~1900 A/cm^2 are plotted in Fig. 5(a). The position and intensity of the peaks were extracted and are presented in Fig. 5(b). As the peaks of the MQW shift toward the measuring edge of the system (~2030 nm), a deviation will exist for the calculated peak position and intensity for temperatures higher than 400 K. Stable operation of GeSn LEDs at a temperature of 460 K is higher than the maximum temperature in silicon integrated circuits [24]. Both MQW and Ge peaks redshift when the operated temperature increases due to the bandgap shrinkage [11]. The shift of the MQW from 300 to 460 K is 27 meV, which is three times the shift of the Ge peak, consistent with previous studies showing that the GeSn LED has a larger shift slope than Ge LED. On the other hand, the opposite trend of the intensity for GeSn and Ge peaks is observed when temperature increases. Both Ge and MQW are indirect band materials. Since there is a 130-meV energy difference between Γ-valley and L-valleys of Ge, the electron is more likely to jump into the Γ-valley at higher temperatures as the distribution is smeared out [34]. Due to the incorporation of Sn, GeSn is closer to direct bandgap materials, resulting in reduced competition between direct and indirect bandgap luminescence. The nonradiative recombination due to the defects from non-equilibrium GeSn growth processes is dominant when the temperature increases [30]. Thus, the method for enhancing the EL intensity of GeSn LEDs from increasing temperature perhaps is unrealistic, as it may occur only on very low Sn content (<4%) GeSn LEDs, which are inefficient [23].

To further study the band structure and emission characteristics of GeSn/Ge MQW LEDs, PL spectra as a function of temperature (220–460 K) were measured on a device using the PL system with a laser at the wavelength of 532 nm.

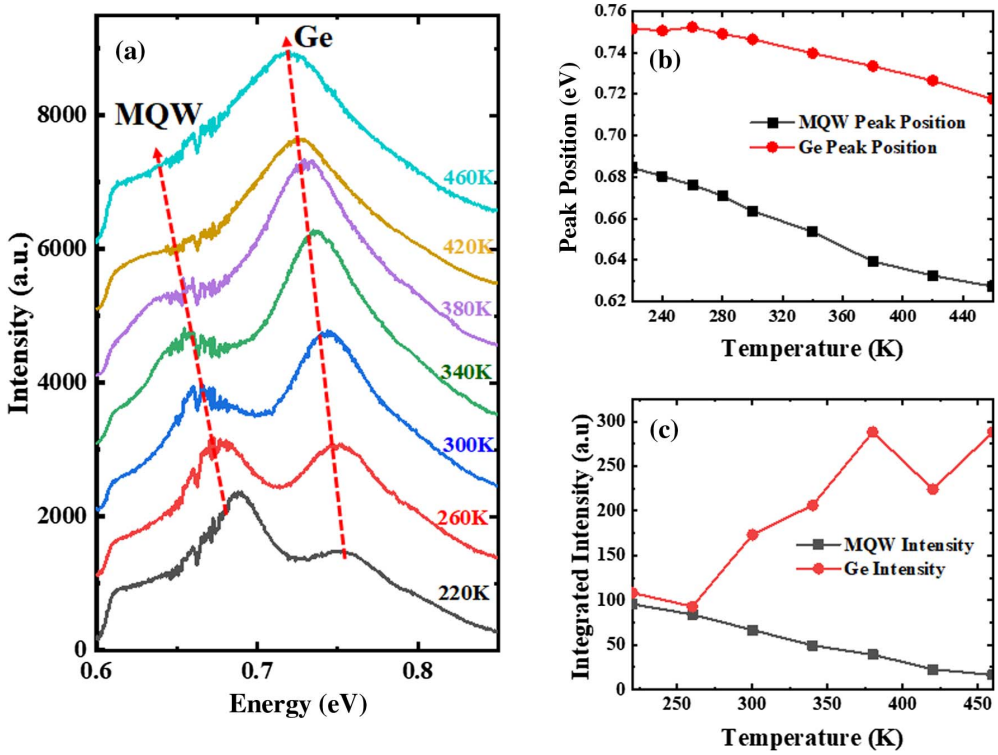

Fig. 6. (a) PL spectra as a function of temperature; (b), (c) peak position and PL integrated intensity at temperature from 220 to 460 K.

As shown in Fig. 6(a), two dominant PL peaks exist, which are along the emission from the direct band of GeSn (MQW) and Ge. The energies of GeSn and Ge peaks at 300 K are around 0.664 eV (1867 nm) and 0.746 eV (1662 nm), respectively, which are close to EL peaks 2 and 3 at 0.668 eV (1864 nm) and 0.737 eV (1715 nm) with a low injection current at 1 mA in Fig. 4. The peak of Ge is a slight redshift compared to the common as-grown Ge layer (~1580–1600 nm) with a 0.2% tensile strain, which might be due to the n-type doping on the n-contact layer. The incorporation of n-type dopants in Ge allows for raising the Fermi level, which reduces the energy of the direct band [35]. The redshift of both peaks from increasing temperature is consistent with the above temperature-dependent EL analysis. Additionally, the PL GeSn peak also has a larger shift slope than the PL Ge peak [Fig. 6(b)]. Finally, the opposite temperature-dependent trend of the PL intensity of GeSn and Ge peaks aligns well with the previous EL analysis [Fig. 6(c)].

3. CONCLUSION

We present the first GeSn/Ge MQW LEDs on a 12-inch (300 mm) diameter Si wafer. The LEDs were grown on Si by commercial RPCVD, showing great potential for large-scale manufacturing. The integrated EL intensity of the GeSn MQW LED is 27.58 times that of the Ge LED, due to the reduced bandgap difference between indirect and direct bands. The GeSn LED has a dominant peak near 0.665 eV (1864 nm), consistent with the theoretical calculation of ~0.660 eV for the direct bandgap of GeSn well. The emission of the GeSn LED covers a wide range from 0.65 to 0.85 eV (1458–2066 nm), which covers the S, O, L, U, and 2-μm optical communication bands. The stable operation of GeSn LEDs at a temperature of 460 K is higher than the maximum temperature in silicon integrated circuits. Finally, the temperature-dependent EL/PL spectra also show the opposite integrated intensity trend of GeSn and Ge peaks, indicating the aggravated nonradiative recombination for GeSn emission. This work shows that GeSn/Ge MQW emitters are potential group-IV light sources for large-scale manufacturing.

Funding. CAS Project for Young Scientists in Basic Research (YSBR-026); National Research Foundation Singapore under its Competitive Research Program (NRF-CRP19-2017-01); Ministry of Education - Singapore AcRF Tier 2 (T2EP50121-0001 (MOE-000180-01)); Ministry of Education - Singapore AcRF Tier 1 (2021-T1-002-031 (RG112/21)).

Acknowledgment. We thank Nanyang NanoFabrication Centre (N2FC) for the use of semiconductor process equipment.

Disclosures. The authors declare no conflicts of interest.

Data Availability. The data that support the findings of this study are available from the corresponding authors upon reasonable request.

REFERENCES

1. P. Chaisakul, D. Marris-Morini, J. Frigerio, D. Chrastina, M.-S. Rouifed, S. Cecchi, P. Crozat, G. Isella, and L. Vivien, "Integrated germanium optical interconnects on silicon substrates," Nat. Photonics **8**, 482–488 (2014).
2. J. Liu, X. Sun, R. Camacho-Aguilera, L. C. Kimerling, and J. Michel, "Ge-on-Si laser operating at room temperature," Opt. Lett. **35**, 679–681 (2010).
3. R. Geiger, T. Zabel, and H. Sigg, "Group IV direct band gap photonics: methods, challenges, and opportunities," Front. Mater. **2**, 52 (2015).
4. Z. Wang, A. Abbasi, U. Dave, A. De Groote, S. Kumari, B. Kunert, C. Merckling, M. Pantouvaki, Y. Shi, B. Tian, K. Van Gasse, J. Verbist, R. Wang, W. Xie, J. Zhang, Y. Zhu, J. Bauwelinck, X. Yin, Z. Hens, J. Van Campenhout, B. Kuyken, R. Baets, G. Morthier, D. Van Thourhout, and G. Roelkens, "Novel light source integration approaches for silicon photonics," Laser Photon. Rev. **11**, 1700063 (2017).
5. Y. Zhou, Y. Miao, S. Ojo, H. Tran, G. Abernathy, J. M. Grant, S. Amoah, G. Salamo, W. Du, J. Liu, J. Margetis, J. Tolle, Y.-H. Zhang, G. Sun, R. A. Soref, B. Li, and S.-Q. Yu, "Electrically injected GeSn lasers on Si operating up to 100 K," Optica **7**, 924–928 (2020).
6. K. P. Homewood and M. A. Lourenço, "The rise of the GeSn laser," Nat. Photonics **9**, 78–79 (2015).
7. O. Moutanabbir, S. Assali, X. Gong, E. O'Reilly, C. Broderick, B. Marzban, J. Witzens, W. Du, S.-Q. Yu, A. Chelnokov, D. Buca, and D. Nam, "Monolithic infrared silicon photonics: the rise of (Si)GeSn semiconductors," Appl. Phys. Lett. **118**, 110502 (2021).
8. A. Elbaz, D. Buca, N. von den Driesch, K. Pantzas, G. Patriarche, N. Zerounian, E. Herth, X. Checoury, S. Sauvage, I. Sagnes, A. Foti, R. Ossikovski, J.-M. Hartmann, F. Boeuf, Z. Ikonic, P. Boucaud, D. Grützmacher, and M. El Kurdi, "Ultra-low-threshold continuous-wave and pulsed lasing in tensile-strained GeSn alloys," Nat. Photonics **14**, 375–382 (2020).
9. J. Chrétien, N. Pauc, F. Armand Pilon, M. Bertrand, Q.-M. Thai, L. Casiez, N. Bernier, H. Dansas, P. Gergaud, E. Delamadeleine, R. Khazaka, H. Sigg, J. Faist, A. Chelnokov, V. Reboud, J.-M. Hartmann, and V. Calvo, "GeSn lasers covering a wide wavelength range thanks to uniaxial tensile strain," ACS Photon. **6**, 2462–2469 (2019).
10. D. Buca, A. Bjelajac, D. Spirito, O. Concepción, M. Gromovyi, E. Sakat, X. Lafosse, L. Ferlazzo, N. von den Driesch, Z. Ikonic, D. Grützmacher, G. Capellini, and M. El Kurdi, "Room temperature lasing in GeSn microdisks enabled by strain engineering," Adv. Opt. Mater. **10**, 2201024 (2022).
11. L. Peng, X. Li, Z. Liu, X. Liu, J. Zheng, C. Xue, Y. Zuo, and B. Cheng, "Horizontal GeSn/Ge multi-quantum-well ridge waveguide LEDs on silicon substrates," Photon. Res. **8**, 899–903 (2020).
12. L. Peng, X. Li, J. Zheng, X. Liu, M. Li, Z. Liu, C. Xue, Y. Zuo, and B. Cheng, "Room-temperature direct-bandgap electroluminescence from type-I GeSn/SiGeSn multiple quantum wells for 2 μm LEDs," J. Lumin. **228**, 117539 (2020).
13. D. Stange, N. von den Driesch, D. Rainko, S. Roesgaard, I. Povstugar, J.-M. Hartmann, T. Stoica, Z. Ikonic, S. Mantl, D. Grützmacher, and D. Buca, "Short-wave infrared LEDs from GeSn/SiGeSn multiple quantum wells," Optica **4**, 185–188 (2017).
14. P. F. Ambrico, A. Amodeo, P. Di Girolamo, and N. Spinelli, "Sensitivity analysis of differential absorption lidar measurements in the mid-infrared region," Appl. Opt. **39**, 6847–6865 (2000).
15. P. J. Roberts, F. Couny, H. Sabert, B. J. Mangan, D. P. Williams, L. Farr, M. W. Mason, A. Tomlinson, T. A. Birks, J. C. Knight, and P. St. J. Russell, "Ultimate low loss of hollow-core photonic crystal fibres," Opt. Express **13**, 236–244 (2005).
16. H. Zhang, Z. Li, N. Kavanagh, J. Zhao, N. Ye, Y. Chen, N. V. Wheeler, J. Wooler, J. R. Hayes, S. R. Sandoghchi, F. Poletti, M. N. Petrovich, S. U. Alam, R. Phelan, J. O'Carroll, B. Kelly, D. J. Richardson, B. Corbett, and F. C. Garcia Gunning, "81 Gb/s WDM transmission at 2 μm over 1.15 km of low-loss hollow core photonic bandgap fiber," in *European Conference on Optical Communication (ECOC)* (2014), pp. 1–3.

17. S. Wu, S. Xu, H. Zhou, Y. Jin, Q. Chen, Y.-C. Huang, L. Zhang, X. Gong, and C. S. Tan, "High-performance back-illuminated $Ge_{0.92}Sn_{0.08}$/Ge multiple-quantum-well photodetector on Si platform for SWIR detection," IEEE J. Sel. Top. Quantum Electron. **28**, 8200109 (2022).
18. X. Li, L. Peng, Z. Liu, Z. Zhou, J. Zheng, C. Xue, Y. Zuo, B. Chen, and B. Cheng, "30 GHz GeSn photodetector on SOI substrate for 2 μm wavelength application," Photon. Res. **9**, 494–500 (2021).
19. S. Xu, W. Wang, Y.-C. Huang, Y. Dong, S. Masudy-Panah, H. Wang, X. Gong, and Y.-C. Yeo, "High-speed photo detection at two-micron-wavelength: technology enablement by GeSn/Ge multiple-quantum-well photodiode on 300 mm Si substrate," Opt. Express **27**, 5798–5813 (2019).
20. H. Li, Y. X. Cui, K. Y. Wu, W. K. Tseng, H. H. Cheng, and H. Chen, "Strain relaxation and Sn segregation in GeSn epilayers under thermal treatment," Appl. Phys. Lett. **102**, 251907 (2013).
21. P. Zaumseil, Y. Hou, M. Schubert, N. Von Den Driesch, D. Stange, D. Rainko, M. Virgilio, D. Buca, and G. Capellini, "The thermal stability of epitaxial GeSn layers," APL Mater. **6**, 076108 (2018).
22. S. Wu, B. Son, L. Zhang, Q. Chen, H. Zhou, S. C. K. Goh, and C. S. Tan, "Effects of high-temperature thermal annealing on GeSn thin-film material and photodetector operating at 2 μm," J. Alloy. Compd. **872**, 159696 (2021).
23. B.-J. Huang, C.-Y. Chang, Y.-D. Hsieh, R. A. Soref, G. Sun, H.-H. Cheng, and G.-E. Chang, "Electrically injected GeSn vertical-cavity surface emitters on silicon-on-insulator platforms," ACS Photon. **6**, 1931–1938 (2019).
24. M. A. Huque, S. K. Islam, B. J. Blalock, C. Su, R. Vijayaraghavan, and L. M. Tolbert, "Silicon-on-insulator based high-temperature electronics for automotive applications," in *IEEE International Symposium on Industrial Electronics* (2008), pp. 2538–2543.
25. H. Zhou, S. Xu, S. Wu, Y.-C. Huang, P. Zhao, J. Tong, B. Son, X. Guo, D. Zhang, X. Gong, and C. S. Tan, "Photo detection and modulation from 1550 to 2000 nm realized by a GeSn/Ge multiple-quantum-well photodiode on a 300-mm Si substrate," Opt. Express **28**, 34772–34786 (2020).
26. C.-H. Tsai, B.-J. Huang, R. A. Soref, G. Sun, H. H. Cheng, and G.-E. Chang, "GeSn resonant-cavity-enhanced photodetectors for efficient photodetection at the 2 μm wavelength band," Opt. Lett. **45**, 1463–1466 (2020).
27. H. Cong, C. Xue, J. Zheng, F. Yang, K. Yu, Z. Liu, X. Zhang, B. Cheng, and Q. Wang, "Silicon based GeSn pin photodetector for SWIR detection," IEEE Photon. J. **8**, 7563433 (2016).
28. Y. Lin, B. Son, K. H. Lee, J. Michel, and C. S. Tan, "Sub-mA/cm^2 dark current density, buffer-less germanium (Ge) photodiodes on a 200-mm Ge-on-insulator substrate," IEEE Trans. Electron Devices **68**, 1730–1737 (2021).
29. E. Kasper and M. Oehme, "Germanium tin light emitters on silicon," Jpn. J. Appl. Phys. **54**, 04DG11 (2015).
30. D. Stange, N. von den Driesch, D. Rainko, C. Schulte-Braucks, S. Wirths, G. Mussler, A. T. Tiedemann, T. Stoica, J. M. Hartmann, Z. Ikonic, S. Mantl, D. Grützmacher, and D. Buca, "Study of GeSn based heterostructures: towards optimized group IV MQW LEDs," Opt. Express **24**, 1358–1367 (2016).
31. B. Schwartz, M. Oehme, R. Koerner, S. Bechler, J. Schulze, and M. Kittler, "Luminescence of strained Ge on GeSn virtual substrate grown on Si (001)," Proc. SPIE **10108**, 101080D (2017).
32. B. Schwartz, A. Klossek, M. Kittler, M. Oehme, E. Kasper, and J. Schulze, "Electroluminescence of germanium LEDs on silicon: influence of antimony doping," Phys. Status Solidi C **11**, 1686–1691 (2014).
33. J. P. Gupta, N. Bhargava, S. Kim, T. Adam, and J. Kolodzey, "Infrared electroluminescence from GeSn heterojunction diodes grown by molecular beam epitaxy," Appl. Phys. Lett. **102**, 251117 (2013).
34. T.-H. Cheng, C.-Y. Ko, C.-Y. Chen, K.-L. Peng, G.-L. Luo, C. W. Liu, and H.-H. Tseng, "Competitiveness between direct and indirect radiative transitions of Ge," Appl. Phys. Lett. **96**, 091105 (2010).
35. X. Sun, J. Liu, L. C. Kimerling, and J. Michel, "Direct gap photoluminescence of n-type tensile-strained Ge-on-Si," Appl. Phys. Lett. **95**, 011911 (2009).